

A FLANGED PARALLEL-PLATE WAVEGUIDE PROBE FOR MICROWAVE IMAGING OF TUMORS

H. Zhang, S. Y. Tan, and H. S. Tan

School of Electrical and Electronic Engineering
Nanyang Technological University
Singapore 639798, Singapore

Abstract—This paper presents a microwave imaging method for malignant tumors using flanged parallel-plate waveguide probes, based on detecting the significant difference in complex permittivity that exists between the tumor and its surrounding tissues. The presence of a tumor is identified from a frequency scan of the resonant scattering parameters. The tumor location can be estimated using S_{21} obtained at various positions of the region of concern, e.g., human organ, biological tissues, etc., while another probe transmits at the position yielding maximum resonating response of S_{11} , with triangulation technique. A tumor can also be distinguished from clutter items. With specific reference to the detection of breast cancer, simulation studies are presented to verify the performance of this probe and the proposed detection technique.

1. INTRODUCTION

Cancer is the leading cause of deaths worldwide. By 2030 it is predicted more than 26 million people are diagnosed with cancer [1]. WHO has also projected in the year 2030, there would be a 12 million global cancer deaths [2]. With the increase in life expectancy, incidence of cancer and associated death rates are expected to remain high as risk increases dramatically with age. However, reduction in mortality rates for cancer can be made possible. More than 30% of the cancer deaths rate could be decreased as cancers can be cured if detected and treated early [1, 2]. Thus early cancer screening takes on a vital role in reducing this public burden as treatment is more effective when cancer is detected earlier. However, available screening programmes may be costly and more cumbersome to use, such as magnetic resonance

Corresponding author: S. Y. Tan (esytan@ntu.edu.sg).

imaging (MRI) and positron emission tomography (PET). Even the widely accepted mammography for breast cancer detection also has its limitations, take for instance its high false positive and negative rates [3, 4], and patient's exposure to ionizing radiation and painful breast compression.

In view of this, microwave imaging based on detecting the difference in complex permittivity between a malignant tumor and the surrounding healthy tissues, including systems such as the ultra-wide band (UWB) radar-based [5–12] and microwave tomography [13–15], has been explored as a new modality for tumor detection that can that overcome the current limitations of the screening methods. In addition to above mentioned techniques, a flanged parallel-plate waveguide probe (PPWP) has also been proposed as a device for microwave imaging [16]. This device may be applied to detection of cancers where the tumor differs significantly in electrical properties from its host medium. The PPWP functions as the microwave source radiating into the region of concern. A tumor exhibiting dielectric properties in high contrast to the healthy tissue alters the S_{11} , hence the presence of tumor is identified by significant resonance in the S_{11} or reflection coefficient at the aperture of the PPWP. Clutter items having lower dielectric contrast compared to the tumor can be used to distinguish from the latter with the resonant magnitude. An estimate of the size and location of the tumor can also be derived from the resonant S_{11} .

In the previous works, the tumor is assumed to be positioned along the axis of the PPWP; and the depth of the tumor located is estimated from the calibrated amplitudes of $\Delta\Gamma$, the difference in S_{11} between from a tumor and that from normal tissue, as the received signal depends on the tumor's location [16]. However, the effectiveness of this method to localize the tumor may be impacted by any slight changes in the tissue properties. Attenuation due to these variations in tissue properties affects the accuracy of estimating the depth of the embedded tumor using these calibrated amplitudes of the backscattered signal. Thus, we propose an enhanced technique using the PPWP for both S_{11} and S_{21} measurements, which can detect an arbitrary position of the tumor. Over and above the additional information of S_{21} helps to improve the accuracy of locating the tumor as slight variation in tissue properties is insignificant with the use of triangulation technique.

In what follows, Section 2 provides a review of the formulation of the problem, including the expressions of scattered signals in terms of S parameters in the presence of a tumor. The enhanced methodology will be described in details with specific reference to the detection of breast cancer in Section 3, while simulation studies are presented in

Section 4 to illustrate the potential of this method. Lastly, Section 5 summarizes the conclusion.

2. FORMULATION

For the simplicity of analysis, the PPWP with transverse electric and magnetic (TEM) mode waves propagating is of width $2a$, infinite in extent in the y -axis with flanges extending infinitely in both the x - and y -axes, as shown in Fig. 1. Throughout the paper, the time harmonic variation of $e^{-i\omega t}$ is assumed and suppressed.

2.1. Radiated Fields

With the PPWP as the microwave source, the radiated electric fields into Region III (breast tissue, in the case of breast cancer detection), E_x^{III} and E_z^{III} , can be represented respectively as [16, 17]

$$E_x^{III}(x, z) = \frac{1}{2\pi} \int_{-\infty}^{\infty} \frac{k_{z3}}{\omega\epsilon_3} \tilde{H}_{III}^+(\zeta, 0) e^{-i\zeta x + ik_{z3}z} d\zeta \quad (1)$$

$$E_z^{III}(x, z) = \frac{1}{2\pi} \int_{-\infty}^{\infty} \frac{\zeta}{\omega\epsilon_3} \tilde{H}_{III}^+(\zeta, 0) e^{-i\zeta x + ik_{z3}z} d\zeta \quad (2)$$

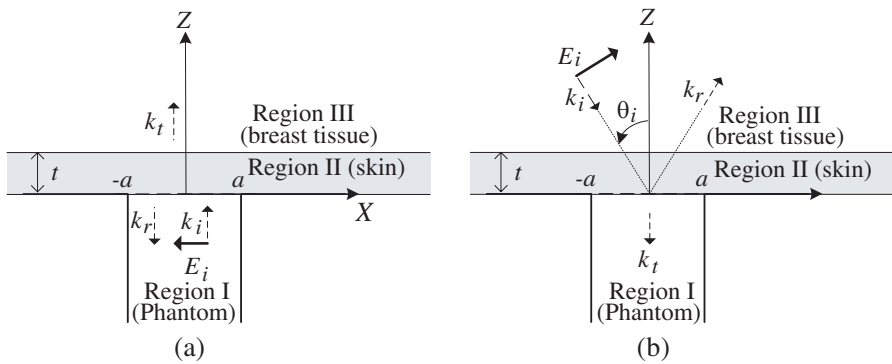


Figure 1. Geometry of the PPWP. (a) Probe Radiating. (b) Probe Receiving.

where the magnetic field in the spectral domain ζ , $\tilde{H}_{III}^+(\zeta, 0)$, is found to be

$$\begin{aligned} \tilde{H}_{III}^+(\zeta, 0) = & e^{i(k_{z2}-k_{z3})t} \left(1 + \frac{\varepsilon_3 k_{z2} - \varepsilon_2 k_{z3}}{\varepsilon_3 k_{z2} + \varepsilon_2 k_{z3}} \right) \left(\frac{1}{1-\alpha} \right) \\ & \frac{\varepsilon_2}{\varepsilon_1} \left[H_0^I \xi_0 K_0(\zeta) - \sum_{m=0}^{\infty} c_m \xi_m K_m(\zeta) \right] \end{aligned} \quad (3)$$

H_0^I is the amplitude of the incident magnetic field with wave number k_1 in the guide (Region I).

And,

$$k_{z2} = \sqrt{k_2^2 - \zeta^2}, \quad k_{z3} = \sqrt{k_3^2 - \zeta^2}$$

where k_2 and k_3 are the wave numbers in the Region II (skin) and Region III respectively.

The other variables are defined as follows

$$\alpha = e^{i2k_{z2}t} \left(\frac{\varepsilon_3 k_{z2} - \varepsilon_2 k_{z3}}{\varepsilon_3 k_{z2} + \varepsilon_2 k_{z3}} \right) \quad (4)$$

$$K_m(\zeta) = \frac{-i\zeta}{k_{z2}(\zeta^2 - a_m^2)} \left[e^{i\zeta a} (-1)^m - e^{-i\zeta a} \right] \quad (5)$$

$$a_m = \frac{m\pi}{2a} \quad (6)$$

$$\xi_m = \sqrt{k_1^2 - a_m^2}. \quad (7)$$

Upon matching the boundary conditions, the coefficients c_m in (3) can be solved from

$$\frac{\varepsilon_2}{\varepsilon_1} \left[H_0^I \xi_0 J_{0n} - \sum_{m=0}^{\infty} \xi_m c_m J_{mn} \right] = 2\pi a (H_0^I \delta_{n0} + c_n) \psi_n \quad (8)$$

where δ_{mn} represents the Kronecker delta, $\psi_0 = 2$, $\psi_1 = \psi_2 = \dots = 1$, and

$$J_{mn} = \int_{-\infty}^{\infty} \left(\frac{1+\alpha}{1-\alpha} \right) \frac{\zeta^2 [(-1)^m e^{i\zeta a} - e^{-i\zeta a}] [(-1)^n e^{-i\zeta a} - e^{i\zeta a}]}{k_{z2}(\zeta^2 - a_m^2)(\zeta^2 - a_n^2)} d\zeta. \quad (9)$$

E_x^{III} and E_z^{III} are the fields incident on the tumor (if any). In addition, at the aperture of the PPWP, the reflection coefficient (for healthy tissues in the absence of tumor) is given by

$$\Gamma_0(\omega) = -\frac{c_0}{H_0^I}. \quad (10)$$

2.2. Receiving Characteristic

To derive a simplified solution for the receiving characteristic of the PPWP, it is assumed the scattered field from the scatterer arriving at the aperture is locally plane. Assuming a plane wave emanating from Region III at oblique incidence at the aperture of the PPWP, the receiving characteristic (or transmission coefficient at the aperture), $\tau_0(\theta_i, \omega)$, can be obtained from the following expression [16]

$$\sum_{m=0}^{\infty} \frac{\varepsilon_2}{\varepsilon_1} \xi_m b_m J_{mn} = 2\pi \left(\frac{4H_0^{III} \varepsilon_2 k_z}{\varepsilon_3 \sqrt{k_2^2 - \kappa_x^2} + \varepsilon_2 k_z} L_n - a \psi_n b_n \right) \left(-e^{i2k_{z2}t} (\varepsilon_3 \sqrt{k_2^2 - k_x^2} + \varepsilon_2 k_z) \right) \quad (11)$$

where

$$k_x = k_3 \sin \theta_i \quad (12)$$

$$k_z = k_3 \cos \theta_i \quad (13)$$

and

$$L_n = \frac{ik_x [(-1)^n e^{ik_x a} - e^{-ik_x a}]}{a_n^2 - k_x^2} \quad (14)$$

with H_0^{III} as the amplitude of the incident magnetic field in Region III; $k_2, k_3, k_{z2}, \xi_m, a_m, \psi_n, J_{mn}$ are as defined earlier.

Solving for the coefficients $b_m, \tau_0(\theta_i, \omega)$ can hence be found to be

$$\tau_0 = \frac{b_0}{H_0^{III}}. \quad (15)$$

The employment of τ_0 and the previously found Γ_0 would be covered in detail in the following.

2.3. Scattering Parameters

The basis of the detection technique is the Mie scattering of dielectric bodies [18]. It is assumed the incident field onto the small spherical tumor embedded in the tissue is locally plane. For a plane wave with amplitude E_0 polarized in the x'_1 -direction propagating in the negative z'_1 -direction as defined in Fig. 2, that is

$$E^{inc} = E_0 \hat{a}_{x'_1} e^{-ik_3 z'_1} \quad (16)$$

the scattered electric field at a point $P (r'_1, \theta'_1, \phi'_1)$ outside the sphere takes the form of

$$E^s(P, \omega) = E_0 \frac{e^{ik_3 r'_1}}{k_3 r'_1} \left[\cos \phi'_1 S_1(\theta'_1) \hat{a}_{\theta'_1} - \sin \phi'_1 S_2(\theta'_1) \hat{a}_{\phi'_1} \right] \quad (17)$$

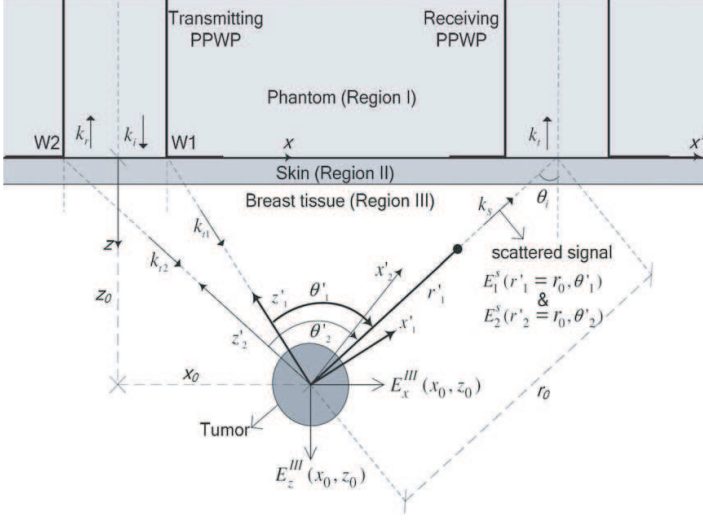


Figure 2. Vertical cross-sectional view of a PPWP radiating into a breast tissue and receiving the backscattered signal from the tumor. Another PPWP receives the scattered signal from the tumor.

where

$$S_1(\theta'_1) = \sum_{n=1}^{\infty} (-i)^{n+1} \left[A_n \frac{P_n^1(\cos \theta'_1)}{\sin \theta'_1} + iB_n \frac{d}{d\theta'_1} P_n^1(\cos \theta'_1) \right] \quad (18)$$

and

$$S_2(\theta'_1) = \sum_{n=1}^{\infty} (-i)^{n+1} \left[A_n \frac{d}{d\theta'_1} P_n^1(\cos \theta'_1) + iB_n \frac{P_n^1(\cos \theta'_1)}{\sin \theta'_1} \right] \quad (19)$$

with the coefficients of the Mie solution given as

$$A_n = (-i)^n \frac{2n+1}{n(n+1)} \left[\frac{j_n(k_3 r_0) [k_4 r_0 j_n(k_4 r_0)]' - j_n(k_4 r_0) [k_3 r_0 j_n(k_3 r_0)]'}{j_n(k_4 r_0) [k_3 r_0 h_n^{(1)}(k_3 r_0)]' - h_n^{(1)}(k_3 r_0) [k_4 r_0 j_n(k_4 r_0)]'} \right] \quad (20)$$

$$B_n = (-i)^{n+1} \frac{2n+1}{n(n+1)} \left[\frac{j_n(k_3 r_0) [k_4 r_0 j_n(k_4 r_0)]' - m_4^2 j_n(k_4 r_0) [k_3 r_0 j_n(k_3 r_0)]'}{h_n^{(1)}(k_3 r_0) [k_4 r_0 j_n(k_4 r_0)]' - m_4^2 j_n(k_4 r_0) [k_3 r_0 h_n^{(1)}(k_3 r_0)]'} \right] \quad (21)$$

k_4 denotes the wave number of the sphere, defined as

$$k_4 = \omega \sqrt{\varepsilon_4 \mu_0} = \omega \sqrt{(\varepsilon_4' + i\varepsilon_4'')\mu_0} = k_3 m_4 \quad (22)$$

and the primes []' denote differentiation with respect to the argument $k_3 r_0$ or $k_4 r_0$.

Using uniform geometrical theory of diffraction (UTD) [19, 20], it can be proven that at a field point (x_0, z_0) in Region III is illuminated by the fields diffracted from the two wedges of the PPWP at W_1 and W_2 as shown in Fig. 2. In the directions from W_1 and W_2 , resolving the fields $E_x^{III}(x_0, z_0)$ and $E_z^{III}(x_0, z_0)$ incident on the tumor result in two contributions of scattered field $E_1^s(r_1', \theta_1', \omega)$ and $E_2^s(r_2', \theta_2', \omega)$. By the superposition of the two, the effective scattered signal E^s is found.

In this manner, the scattered signal in terms of S_{11} and S_{21} in the presence of a tumor would be expressed respectively as

$$S_{11} = \frac{E_x^r + \tau_0 E_x^s}{E_x^i} = \Gamma_0 + \Delta\Gamma \quad (23)$$

and

$$S_{21} = \frac{\tau_0 E_x^s}{E_x^i} = \Delta\Gamma \quad (24)$$

where

$$\Delta\Gamma = \frac{\tau_0 [E_1^s(r_1' = r_0, \theta_1', \omega) + E_2^s(r_2' = r_0, \theta_2', \omega)]}{E_x^i} \quad (25)$$

E_x^i is the incident field at the aperture of the PPWP; the probe characteristic τ_0 is dependent on the angle θ_i , and can be derived using (15).

To simplify the analysis, the scattered electric field from the scatterer into the aperture of the PPWP is assumed to be plane wave.

3. METHODOLOGY

In a method corresponding to that highlighted in [16], the PPWP is to be scanned around the region of concern, e.g., human organ or biological tissues, etc., making S_{11} measurements at different positions. The PPWP is to be immersed in a skin-mimicking phantom to minimize reflections which can arise due to interfaces between different mediums. By performing N measurements, ${}^N C_2$ numbers of ΔS_{11} (differences in S_{11}) can be obtained. Resonant ΔS_{11} with respect to frequency and amplitude indicates one of the pair of S_{11} measurements contains the backscattered signal from the tumor, that is one of the measurements is made at a position near the tumor. On the contrary, an absence of resonance indicates there is no tumor present at the

positions where the pair of measurements is obtained. Furthermore, using the resonant scattered signal and its amplitude, a tumor can be distinguished from clutter items of a lower dielectric constant than the tumor. This is attributed by the fact that the larger the difference in dielectric properties exists between the scatterer and the surrounding medium, the larger is the scattered signal.

In using the previously proposed method of utilising calibrated amplitudes of $\Delta\Gamma$ to estimate the position of the tumor [16], inaccuracies may arise due to attenuation of the backscattered signals resulted by slight changes in tissue properties. To overcome this, an enhanced technique is proposed. After obtaining ${}^N C_2$ numbers of ΔS_{11} from the N measurements, the region which is believed to have a tumor embedded beneath is identified by eliminating the positions that yields non-resonant ΔS_{11} . Using the detection of breast cancer as an illustration of this proposed method, with reference to Fig. 3, to zoom into the position where the tumor is located, the PPWP is to be scanned about this region (Region 2 in the figure) to obtain the maximum resonating response of ΔS_{11} (the difference between S_{11} measurement from Region 1 (no tumor present) and that from Region 2). The tumor is closest to the final position with the maximum ΔS_{11} .

Additionally, one of the PPWP is used to make measurements at different positions of the breast, receiving scattered signals in terms of S_{21} , while another PPWP is fixed as the transmitting probe at the position yielding maximum resonating ΔS_{11} . In the presence of a

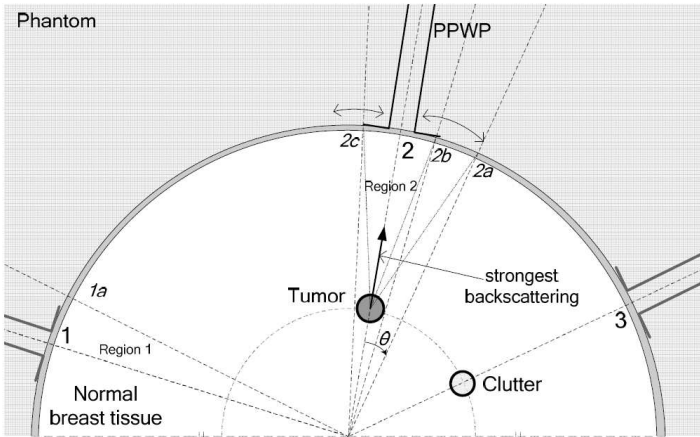


Figure 3. Scanning a PPWP about the breast for maximum resonating response of S_{11} .

scatterer, there exist positions where amplitude of S_{21} is minimum as the receiving PPWP is scanned around the breast. In accordance with the Mie's Theory, typically the scattered signal is weakest at 90° from the direction of propagation of the incident field. Hence the position at which the minimum S_{21} occurs is approximately $\theta'_1 = \pm 90^\circ$ from the transmitting PPWP (see Fig. 4, assuming the probes are in the same plane). It is hence possible to use triangulation technique to determine the depth of the tumor embedded beneath the transmitting PPWP.

Consider a unit electric field incident on a tumor of diameter 5 mm, having dielectric contrast $5 - j0.2$ from the surrounding medium [11, 13].

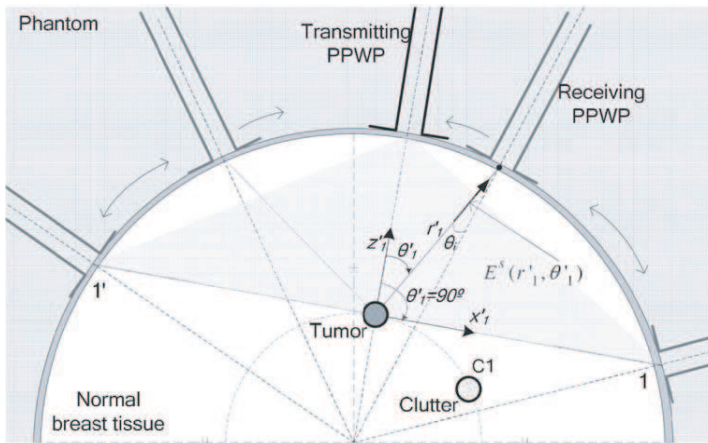


Figure 4. Scanning a PPWP about the breast for minimum response of S_{21} .

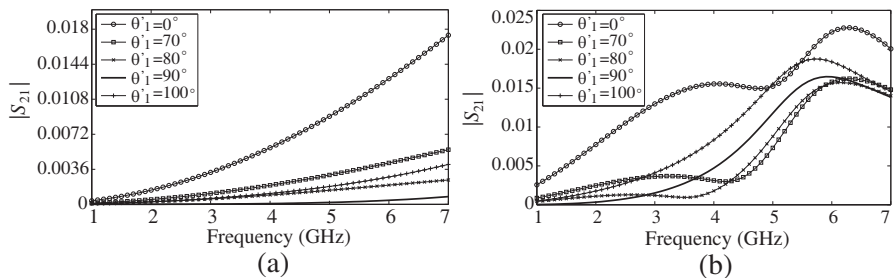


Figure 5. Magnitude of S_{21} at different scattering angle θ'_1 over a frequency range. (a) With dielectric contrast of $5 - j0.2$ between the tumor and the surrounding medium. (b) With dielectric properties defined by (26).

The normalized scattered signal S_{21} at an equidistance of 3 cm at varying scattering angle θ_s is depicted in Fig. 5(a). Minimum S_{21} occurring at $\theta_s = \pm 90^\circ$ is observed.

However, this is not fully in line with the theory, as shown in Fig. 5(b), if the frequency dependence of the dielectric properties of the tissues is modeled using a 2-pole Debye dispersion equation

$$\varepsilon_r(\omega) - j \frac{\sigma(\omega)}{\omega \varepsilon_0} = \varepsilon_\infty + \sum_{p=1}^2 \frac{\varepsilon_{sp} - \varepsilon_\infty}{1 + j\omega\tau_p} \quad (26)$$

where ε_0 is the free space permittivity, and ω is the angular frequency, with Debye parameters to fit the data of the breast tissue for the entire operating frequency range: For skin layer; $\varepsilon_\infty = 4.62$, $\varepsilon_{s1} = 37.10$, $\varepsilon_{s2} = 41.22$, $\tau_1 = 7.51$ ps, $\tau_2 = 0.31$ ns; for normal tissue $\varepsilon_\infty = 2.68$, $\varepsilon_{s1} = 5.01$, $\varepsilon_{s2} = 3.85$, $\tau_1 = 15.84$ ps, $\tau_2 = 0.10$ ns; and for malignant tumor $\varepsilon_\infty = 11.05$, $\varepsilon_{s1} = 51.67$, $\varepsilon_{s2} = 43.35$, $\tau_1 = 8.56$ ps, $\tau_2 = 0.23$ ns [12]. This phenomenon can be explained using (16). The minimum of the sum $S_1(\theta'_1)$ no longer occurs at $\pm 90^\circ$ in the higher frequencies with these dielectric properties defined by the (26). Therefore it is recommended to use operating frequencies of less than 3 GHz in this method of finding minimum S_{21} for triangulation to determine the location of the tumor.

4. NUMERICAL RESULTS AND DISCUSSION

Simulations are performed to demonstrate the effectiveness of the detection method. The PPWP is designed with a width of $2a = 6$ mm for dominant mode wave propagation in 1–7 GHz. Consider a spherical tumor of diameter $d_0 = 5$ mm embedded at a depth h from the surface, in the breast tissue modeled as a concentric hemisphere of radius 50 mm with a skin layer of 2 mm. Included in the breast model are clutter items representing tissue heterogeneity, assumed to have dielectric properties of variation of +30% that of the normal tissue is used [12, 16]. In this study, only the first order scattering from the scatterer is taken into account.

With reference to Fig. 3 where a tumor is embedded at $h = 3$ cm, it is observed as shown in Fig. 6(a), there is resonating $\Delta S_{11(2a,1)}$ (difference between S_{11} obtained at position 2a and position 1 (normal breast tissue)); indicating a tumor is embedded near position 2a. Afterwards, the probe is moved about position 2a until a maximum response of $\Delta S_{11(2,1)}$ is detected at position 2. This implies the tumor is embedded beneath position 2, the reason being within the entire breast, the backscattering is the strongest ($\theta'_1 = 0^\circ$) as can be found

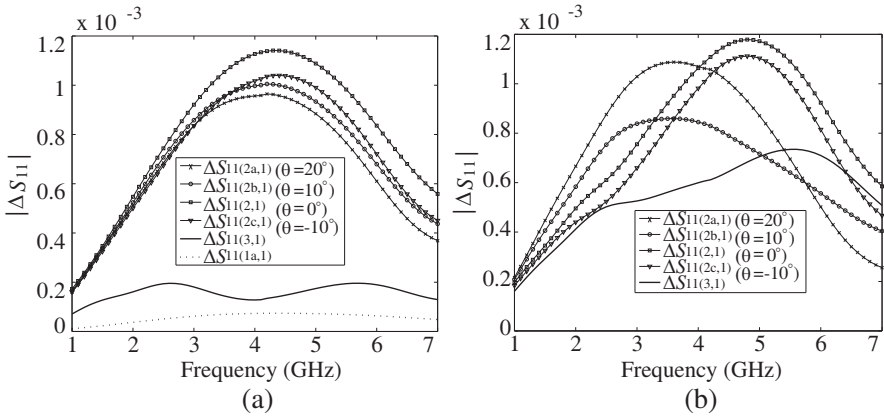


Figure 6. Magnitude of differences ΔS_{21} obtained at various positions of the breast. (a) With clutter assuming 30% dielectric variation of normal breast tissue. (b) With clutter assuming dielectric properties defined by (27).

by (16). Also shown in Fig. 6(a), as the influence of the tumor is minimal in Region 1, $\Delta S_{11(1a,1)}$ (difference between measurements at positions 1 and 1a) does not exhibit any resonating characteristics. In addition, $\Delta S_{11(3,1)}$ displays some resonance but the amplitude is very much weaker than that of ΔS_{11} in Region 2; this is attributed to scattering from the tumor is also picked up at position 3 but the power is lower than that at positions in Region 2. This validates it is possible to zoom into the region where the tumor is located, in this case Region 2.

However, recent studies on the dielectric properties of normal, benign and malignant breast tissues samples in the microwave ultra-wideband range, [21, 22], and the development of anatomically realistic Numerical breast phantoms [23], show that the dielectric contrast between the malignant and normal glandular/fibroconnective tissues in the breast may not be as large as expected, thus presenting a more challenging scenario in microwave imaging of breast tumors. Hence the effects of the clutter assuming dielectric properties of a fibroconnective/glandular tissues report in [23], defined by single-pole Debye dispersive equation:

$$\epsilon_r(\omega) - j\frac{\sigma(\omega)}{\omega\epsilon_0} = \epsilon_\infty + \frac{\epsilon_\Delta - \epsilon_\infty}{1 + j\omega\tau} - j\frac{\sigma_s}{\omega\epsilon_0} \quad (27)$$

with parameters: $\epsilon_\infty = 12.8485$, $\epsilon_\Delta = 24.6430$, $\tau = 13$ ps, $\sigma_s = 0.2514$ S/m, is investigated.

In Fig. 6(b), it is shown that the resonating amplitude of $\Delta S_{11(2,1)}$ is still the maximum with that of $\Delta S_{11(2a,1)}$ is larger than that of $\Delta S_{11(2b,1)}$ due to constructive interferences of both the tumor, and the clutter which has now a larger dielectric contrast (having dielectric constant ranging from 21 to 24 instead of 5 to 8), to the normal breast tissue in this scenario. The amplitude of $\Delta S_{11(2b,1)}$ is still larger than that of $\Delta S_{11(3,1)}$ as scattering from the tumor is still stronger than that from the clutter, thus Region 2 is still identified as the region where the tumor is embedded. In general, larger scatterers result in larger backscattered power; scattered power also increases as the dielectric contrast between the scatterer and host medium increases. Hence it is worthy to note that the challenge to identify this region arises if the dielectric properties of the tumor and clutter become less distinguishable and the size of the clutter increases dramatically.

It has been mentioned earlier that the position at which the minimum S_{21} occurs is approximately $\pm 90^\circ$ from the transmitting PPWP for frequencies less than 3 GHz. In the following example, it is to be validated that using the minimum S_{21} helps to enhance the accuracy of locating the tumor. Recurring the steps involved in obtaining the maximum response of S_{11} described in Section 3, it is found that maximum S_{11} is found at position 2 (see Fig. 4). With a PPWP transmitting at this position at 2 GHz while another PPWP is scanned around the breast, it can be observed in Fig. 7 that in the presence of only a tumor, the minimum S_{21} occurs at $\theta'_1 = \pm 90^\circ$, at positions 1 and 1'. With this knowledge of the position(s) where

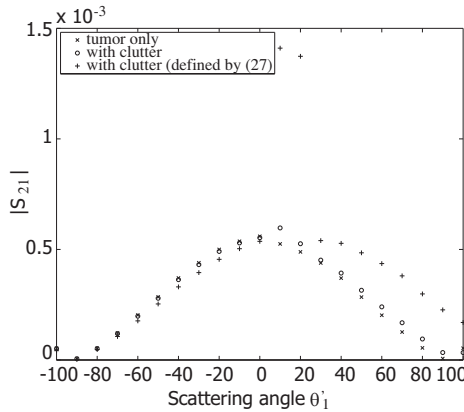


Figure 7. Magnitude of differences ΔS_{21} obtained at different scattering angle θ'_1 at 2 GHz.

minimum S_{21} occur(s), it is possible to use triangulation technique to estimate more accurately the depth of the tumor embedded. It should be noted that if the tumor is embedded at the centre of the hemispheric breast, the result should be symmetrical about $\theta'_1 = 0^\circ$. However, as the tumor is embedded off the centre of the breast towards the right as shown in Fig. 4 in this example, the magnitude of S_{21} is asymmetrical, with magnitude for larger positive θ'_1 is higher than that of the negative θ'_1 as the receiving PPWP is further from the tumor in the latter.

Investigations on how the presence of clutter items affects the S_{21} are also conducted. Having a clutter C_1 having the same size as the tumor, at same depth below the surface of the skin, the S_{21} scanned at the same positions of the breast at 2 GHz is also given in Fig. 7. It is observed that albeit the presence of a clutter, the position where the minimum S_{21} remains as before in the case where only the tumor is present. As can be seen in Fig. 7, as the clutter item is a scatterer itself, there exist constructive and destructive interference at some positions where the receiving PPWP is placed. Nonetheless, as the clutter item is of a lower dielectric contrast (+30% dielectric variations of the normal breast tissue) to the surrounding medium as compared to the tumor, the effect on the position where minimum S_{21} occurs is not significant. With the clutter defined by (25), the position where minimum S_{21} occurs, shifted slightly away from $\theta'_1 = 90^\circ$.

5. CONCLUSION

An enhanced technique for better accuracy of microwave imaging of tumors, on the basis of detecting the difference between the complex permittivity of normal tissue and a malignant tumor or other tissue heterogeneity (clutter items) has been proposed. Using breast cancer detection as an illustration, flanged parallel-plate waveguide probes are employed to perform contact measurements of S_{11} and S_{21} on the breast over a frequency range. The scattered signals have resonating characteristics in the presence of a tumor. Simulation studies show a tumor can be differentiated from a clutter item, within the assumption of there exists a large dielectric contrast between a tumor and the normal breast tissue. On top of this, simulations also illustrated how the depth of the tumor embedded in the breast can be more effectively estimated with the additional information of the S_{21} as a triangulation technique can be employed to locate the tumor from the positions where the minimum S_{21} occur. Recent studies on the dielectric properties of the heterogeneous breast highlighted a challenging scenario for microwave imaging of tumors if the tumor and its host medium do not differ significantly in electrical properties.

Therefore it will be further investigated, modifications to the proposed technique, to identify marginal differences between scattering from a tumor and from its surrounding medium that may possibly occur such as the case of breast cancer.

ACKNOWLEDGMENT

Author Zhang Huiyu gratefully thank the Agency for Science, Technology and Research (A*STAR) of Singapore for providing the A*STAR Graduate Scholarship.

REFERENCES

1. International Union Against Cancer. About Cancer. http://www.uicc.org/index.php?option=com_content&task=view&id=1-3&Itemid=113.
2. World Health Organisation. Cancer Facts. <http://www.who.int/t/mediacentre/factsheets/fs297/en/index.html>.
3. Fletcher, S. W. and J. G. Elmore, "Mammographic screening for breast cancer," *New Engl. J. Med.*, Vol. 37, 1672–1680, 2003.
4. Fear, E. C., P. M. Meaney, and M. A. Stuchly, "Microwaves for breast cancer detection," *IEEE Potentials*, Vol. 22, No. 1, 12–18, February–March 2003.
5. Bindu, G., S. J. Abraham, A. Lonappan, V. Thomas, C. K. Aanandan, and K. T. Mathew, "Active microwave imaging for breast cancer detection," *Progress In Electromagnetics Research*, PIER 58, 149–169, 2006.
6. Guo, B., Y. Wang, and J. Li, "Active imaging via adaptive beamforming methods for breast cancer detection," *Journal of Electromagnetic Waves and Applications*, Vol. 20, No. 1, 53–63, 2006.
7. Kanj, H. and M. Popovic, "A novel ultra-compact broadband antenna for microwave breast tumor detection," *Progress In Electromagnetics Research*, PIER 86, 169–198, 2008.
8. Zainud-Deen, S. H., W. M. Hassen, E. M. Ali, K. H. Awadalla, and H. A. Sharshar, "Breast cancer detection using a hybrid finite difference frequency domain and particle swarm optimization techniques," *Progress In Electromagnetics Research B*, Vol. 3, 35–46, 2008.
9. Amineh, R. K., A. Trehan, and N. K. Nikolova, "TEM horn antenna for ultra-wide band microwave breast imaging," *Progress In Electromagnetics Research B*, Vol. 13, 59–74, 2009.

10. Lim, H. B., T. T. N. Nguyen, E. Li, and D. T. Nguyen, "Confocal microwave imaging for breast cancer detection: Delay-multiply-and-sum image reconstruction algorithm," *IEEE Trans. Biomed. Eng.*, Vol. 55, No. 6, 1697–1704, Jun. 2008.
11. Davis, S. K., B. D. Van Veen, S. C. Hagness, and F. Kelcz, "Breast tumor characterization based on ultrawideband microwave backscatter," *IEEE Trans. Biomed. Eng.*, Vol. 1, 237–246, January 2008.
12. Chen, Y., E. Gunawan, K. S. Low, S. Wang, Y. Kim, and C. B. Soh, "Pulse design for time reversal method as applied to ultrawideband microwave breast cancer detection: A two-dimensional analysis," *IEEE Trans. Antennas Propag.*, Vol. 55, No. 1, 194–204, January 2007.
13. Semenov, S. Y., A. E. Boulyshev, A. Abubakar, V. G. Posukh, Y. Sizov, A. E. Souvorov, P. M. Van den Berg, and T. C. Williams, "Microwave-tomographic imaging of the high dielectric-contrast objects using different image-reconstruction approaches," *IEEE Trans. Microw. Theory Tech.*, Vol. 53, No. 5, 2284–2294, July 2005.
14. Zhou, H., T. Takenaka, J. Johnson, and T. Tanaka, "A breast imaging model using microwaves and a time domain three dimensional reconstruction method," *Progress In Electromagnetics Research*, PIER 93, 57–70, 2009.
15. Drogoudis, D. G., G. A. Kyriacou, and J. N. Sahalos, "Microwave tomography employing an adjoint network based sensitivity matrix," *Progress In Electromagnetics Research*, PIER 94, 213–242, 2009.
16. Zhang, H., S. Y. Tan, and H. S. Tan, "A novel method for breast cancer detection," *Progress In Electromagnetics Research*, PIER 83, 413–434, 2008.
17. Zhang, H., S. Y. Tan, and H. S. Tan, "An improved method for microwave nondestructive dielectric measurement of layered media," *Progress In Electromagnetics Research B*, Vol. 10, 145–161, 2008.
18. Ruck, G. T., D. E. Barrick, W. D. Stuart, and C. K. Krichbaum, *Radar Cross Section Handbook*, Plenum Press, 1970.
19. Ang, T. W., S. Y. Tan, and H. S. Tan, "Analytical methods to determine diffraction points on multiple edges and cylindrical scatterers in UTD ray tracing," *Microw. Opt. Tech. Lett.*, Vol. 22, No. 5, 304–309, 1999.
20. Tan, S. Y. and H. S. Tan, "A microcellular communications propagation model based on uniform theory of diffraction and

- multiple image theory,” *IEEE Trans. Antennas Propag.*, Vol. 44, No. 10, 1310–1326, 1996.
21. Lazebnik, M., D. Popovic, L. McCartney, C. B. Watkins, M. J. Lindstrom, J. Harter, S. Sewall, T. Ogilvie, A. Magliocco, T. M. Breslin, W. Temple, D. Mew, J. H. Booske, M. Okoniewski, and S. C. Hagness, “A large-scale study of the ultrawideband microwave dielectric properties of normal, benign and malignant breast tissues obtained from cancer surgeries,” *Phys. Med. Biol.*, Vol. 52, 6093–6115, 2007.
 22. Lazenik, M., M. Okoniewski, J. H. Booske, and S. C. Hagness, “Highly accurate debye models for normal and malignant breast tissue dielectric properties at microwave frequencies,” *IEEE Microw. Wireless Comp. Lett.*, Vol. 17, No. 12, 822–824, December 2007.
 23. Zastrow, E., S. K. Davis, M. Lazebnik, F. Kelcz, B. D. Van Veen, and S. C. Hagness, “Development of anatomically realistic numerical breast phantoms with accurate dielectric properties for modeling microwave interactions with the human breast,” *IEEE Trans. Biomed. Eng.*, Vol. 55, No. 12, 2792–2800, December 2008.